

Polymer translocation into and out of an ellipsoidal cavity

James M. Polson¹

Department of Physics, University of Prince Edward Island, 550 University Ave., Charlottetown, Prince Edward Island, C1A 4P3, Canada

(Dated: 13 August 2018)

Monte Carlo simulations are used to study the translocation of a polymer into and out of a ellipsoidal cavity through a narrow pore. We measure the polymer free energy F as a function of a translocation coordinate, s , defined to be the number of bonds that have entered the cavity. To study polymer insertion, we consider the case of a driving force acting on monomers inside the pore, as well as monomer attraction to the cavity wall. We examine the changes to $F(s)$ upon variation in the shape anisotropy and volume of the cavity, the polymer length, and the strength of the interactions driving the insertion. For athermal systems, the free energy functions are analyzed using a scaling approach, where we treat the confined portion of the polymer to be in the semi-dilute regime. The free energy functions are used with the Fokker-Planck equation to measure mean translocation times, as well as translocation time distributions. We find that both polymer ejection and insertion is faster for ellipsoidal cavities than for spherical cavities. The results are in qualitative agreement with those of a Langevin dynamics study in the case of ejection but not for insertion. The discrepancy is likely due to out-of-equilibrium conformational behaviour that is not accounted for in the FP approach.

I. INTRODUCTION

Polymer translocation is a fundamental process in which a polymer is transported through a narrow hole in a barrier divides two separate spaces.¹ Over the past two decades, there has been considerable progress in the development of techniques for detecting and monitoring single-molecule translocation events. Much of this work has been motivated by the promise of an efficient and accurate translocation-based method for nucleotide sequencing.²⁻⁵ Other technological applications include protein analysis,⁶ filtration of macromolecules,⁷ and controlled drug delivery.⁸ Polymer translocation is also an important part of numerous biological processes, including viral DNA packaging and ejection, transport of mRNA through the nuclear pore complex, horizontal gene transfer between bacteria, and protein transport across biomembranes.^{9,10} Due to its wide range of applications, polymer translocation has been the subject of numerous theoretical and computer simulation studies in recent years. Much of this work has been summarized in several recent reviews.^{1,11-13}

One important type of polymer translocation involves movement of polymers into or out of confined spaces. Recent theoretical and computer simulation studies in this area have mainly focused on confinement in spherical or ellipsoidal cavities¹⁴⁻³⁷ or laterally unbounded spaces between flat walls.³⁸⁻⁴¹ Much of this work is motivated by the problems of viral DNA packaging and ejection, in which DNA is confined to a space with dimensions comparable to that of its persistence length at near crystalline densities and very high internal pressures. Experimental studies suggest that these processes do not follow simple quasistatic dynamics. For example, ejection proceeds in rapid transient bursts separated by pauses,⁴² while ultra-slow relaxation and nonequilibrium dynamics has been observed during packaging.⁴³ A detailed understanding of these processes using theoretical

methods requires, at a minimum, the use of semi-flexible chain models to account for the high energetic cost of confinement. Numerous studies have examined such models.^{17,18,20-22,25,30,31,34,36,37} On the other hand, such studies are complemented by those that use flexible-chain models to elucidate the specific role of conformational entropy on translocation.^{14-17,19,20,24,26,27,29,31,33,35} Other studies have examined the effects of solvent quality,²² electrostatic interactions,^{25,37} temperature,³⁰ and adsorption to the cavity surface.^{26,27}

A few theoretical studies have considered the effect of cavity shape anisotropy on polymer insertion and ejection.^{20,31,36} Ali *et al.* compared packaging and ejection in ellipsoidal and spherical cavities of equal volume and found that flexible polymers package more quickly in spherical cavities but eject faster in ellipsoidal cavities.²⁰ By contrast, both processes are faster for spherical cavities in the case of semiflexible polymer, leading the authors to suggest this as a reason for the spherical shapes of viruses with pressure-driven ejection. Zhang and Luo recently used a 2-D system to study translocation of a polymer into an elliptical cavity.^{31,36} For flexible chains, they found that the translocation time increased with cavity anisotropy.³¹ In the case of semiflexible polymers, they found that the packaging rate depended the location of the entry point to the cavity, as well as the packing fraction and chain stiffness.³⁶ For a given elliptical cavity at high confinement, they found that entry along the semi-minor axis gave the fastest packaging for sufficiently high stiffness.³⁶

In many simulation studies of polymer translocation into or out of confined spaces, the scaling of the rate of transport with polymer length, N , and cavity dimension, R have been measured. Typically, the results are interpreted using estimates of the confinement free energy, F , of the polymer in the cavity and how it varies with the degree of translocation. The case of polymer ejection from spherical cavities provides a noteworthy illustration. In an early study on the topic, Muthukumar assumed a

scaling $F \sim N/R^{1/\nu}$ to describe the confined portion of the chain, where $\nu \approx 0.588$ is the Flory scaling exponent. This was used to explain the observed scaling of the mean exit time of $\tau \sim N(N/\phi)^{1/3\nu}$, where ϕ is the packing fraction of the cavity for a fully inserted polymer.¹⁴ Subsequently, Cacciuto and Luijten noted that the appropriate scaling of the free energy for triaxial confinement is $F \sim N\phi^{1/(3\nu-1)}$. Using an approach suggested by the scaling of τ for driven translocation given in Ref. 44, they predicted $\tau \sim N^{1+\nu}\phi^{1/(3\nu-1)}$, which was consistent with Monte Carlo (MC) dynamics simulations.¹⁹ Sakaue later questioned the implicit assumption of a constant free energy gradient during translocation and derived an alternative scaling relation that accounts for the decrease and eventual loss of entropic driving force near the end of the process.²³ The scalings observed in each of the MC dynamics studies of Refs. 14 and 19 were shown to be limiting cases of this more general result.

An alternative approach to using analytical estimates of the translocation free energy function is to calculate it explicitly for a chosen model using simulations. Rasmussen *et al.* carried out such calculations for translocation of Lennard-Jones chains into absorbing spherical cavities used the Incremental Gauge Cell MC method.²⁷ The free energy functions were then used in conjunction with the Fokker-Planck (FP) equation to calculate translocation time distributions and probabilities. They observed an interesting non-monotonic dependence of translocation times with a sharp peak located at a local free energy minimum.²⁷ These results were consistent with other results by the same group obtained using self-consistent field theory.²⁶ The validity of the FP approach requires quasistatic conditions during translocation. As noted by Kantor and Kardar⁴⁴ this condition cannot be satisfied for long polymer chains. In addition, nonequilibrium behaviour has been observed in simulations of polymer ejection.³⁵ On the other hand, for sufficiently high pore friction quasistatic translocation is possible and the FP approach is valid.¹ Recently, we used a MC method to calculate translocation free energy functions³² and showed that the predicted translocation time distributions were perfectly consistent with those obtained from dynamics simulations when the pore friction was sufficiently high.^{33,45}

The present work is a theoretical study of the translocation of a flexible polymer into and out of an ellipsoidal cavity. Following our other recent work,^{32,33,45} we use MC simulations to measure the translocation free energy functions. In addition to entropic effects, we also consider the effects of a force located in the nanopore that drives polymer insertion into the cavity. We also consider the effect of monomer attraction to the cavity wall, as in Ref. 27. We examine the effects on the free energy of varying several key system parameters, with special attention to the effects of the anisometry of the cavity. The free energy functions are used with the FP formalism to calculate translocation times for both polymer insertion and ejection. We find that ejection is predicted to be

faster in ellipsoidal cavities in agreement with Ref. 20. Interestingly, we also find that insertion tends to be slower for ellipsoidal cavities, in disagreement with results from that study. This points to the importance of nonequilibrium dynamics, which is not accounted for in the FP approach, as well as the limitations of using free energy functions to predict translocation dynamics.

II. MODEL

We employ a minimal model of a polymer chain that translocates through a narrow pore between an ellipsoidal cavity and semi-infinite space on one side of a flat wall. The polymer is modeled as a flexible chain of N hard spheres, each with a diameter of σ . The pair potential for non-bonded monomers is thus $u_{\text{nb}}(r) = \infty$ for $r \leq \sigma$, and $u_{\text{nb}}(r) = 0$ for $r > \sigma$, where r is the distance between the centers of the monomers. Pairs of bonded monomers interact with a potential $u_{\text{b}}(r) = 0$ if $0.9\sigma < r < 1.1\sigma$, and $u_{\text{b}}(r) = \infty$, otherwise. Consequently, the bond length can fluctuate slightly about its average value. Each monomer interacts with the walls of the system (pore, cavity and barrier) with a hard-particle potential. Thus, the monomer-wall interaction potential is $u_{\text{w}}(r) = 0$ if the distance r between the center of the monomer and the nearest point on the wall satisfies $r > 0.5\sigma$, and $u_{\text{wall}} = \infty$ if $r < 0.5\sigma$. In addition, we consider two different potentials designed to drive the polymer into the cavity. In the first case, monomers that lie inside the pore are subject to a potential described by a constant driving force of magnitude f_{d} that is directed toward the cavity. In the second case, monomers inside the cavity whose centers lie a distance less than σ from the wall have a potential energy of $-\epsilon$ (where $\epsilon > 0$), while all other monomers have zero potential energy.

The pore connecting the cavity to the open space is cylindrical in shape with a diameter D and length L . For most simulations in this study, we choose $D = 1.2\sigma$ and $L = 1.3\sigma$. We choose the z axis to pass through the center of the cylindrical pore. The semi-infinite space on one side of the pore is bounded by an infinite flat wall perpendicular to z . The cavity is an ellipsoid of revolution, with a semi-axis length of a along z and b along x and y . We consider the cases of both prolate ($a > b$) and oblate ($a < b$) ellipsoids, as well as the special case of a spherical cavity ($a = b$). The volume V of the ellipsoid is defined to be the volume of the subspace accessible to the centers of the monomers. This subspace is enclosed by a virtual surface, each point on which lies a distance of 0.5σ from the nearest point on the cavity wall. This virtual surface deviates somewhat from ellipsoidal geometry, except in the special case where $a = b$. The aspect ratio, r , of the cavity is defined to be the ratio of the dimensions of the subspace, i.e. $r = (a - 0.5\sigma)/(b - 0.5\sigma)$. The system is illustrated in Fig. 1.

The degree to which the polymer has translocated across the nanopore into the cavity is quantified using

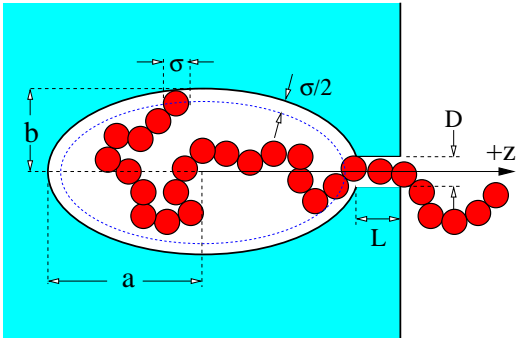


FIG. 1. Illustration of the system studied in this work. The polymer translocates through a cylindrical pore of length L and diameter D between an ellipsoidal cavity of semi-axis lengths of a along z and b along x and y . The near-ellipsoidal space accessible to the monomer centers is shown bounded by the dashed blue line.

a translocation coordinate, s , which is defined in a manner similar to that in a recent study of ours.⁴⁵ It is equal to the number of bonds that have crossed the mid-point of the nanopore. Typically, one bond spans this point for any given configuration, and this bond contributes to s the fraction that lies on the cavity side of the point. This is determined by the z coordinates of the monomers connected by this bond. Note that s is a continuous variable in the range $s \in [0, N - 1]$.

III. FOKKER-PLANCK FORMALISM

We define $\mathcal{W}(s, t; s_0, 0)$ as the probability that a translocating polymer has coordinate s at time t given that it started at s_0 at time $t = 0$. In the quasi-static limit, $\mathcal{W}(s, t; s_0, 0)$ is governed by the Fokker-Planck (FP) equation. In the case where the pore friction is sufficiently strong the equation has the form:¹

$$\frac{\partial \mathcal{W}(s, t; s_0, 0)}{\partial t} = -\frac{\partial J(s, t; s_0, 0)}{\partial s} \quad (1)$$

where the probability flux, $J(s, t; s_0, 0)$ is defined

$$J(s, t; s_0, 0) = -\mathcal{D} \left[\left(\frac{1}{k_B T} \frac{\partial F}{\partial s} \mathcal{W} \right) + \frac{\partial \mathcal{W}}{\partial s} \right], \quad (2)$$

where k_B is Boltzmann's constant and T is temperature. Note that the translocation rate constant \mathcal{D} is independent of s in this limit.

Consider a polymer with a translocation coordinate s_0 at time $t = 0$, where s_0 lies in the domain $s_0 \in [s_a, s_b]$. For $t > 0$, the polymer undergoes stochastic motion governed by \mathcal{D} and $F(s)$ and eventually reaches the domain boundary at $s = s_a$ or $s = s_b$. The first passage time, τ , is the time taken to reach $s = s_b$ for the first time without ever reaching $s = s_a$. The distribution of first

passage times is given by the probability flux at $s = s_b$, i.e.

$$P(\tau) = J(s_b, \tau; s_0, 0), \quad (3)$$

where \mathcal{W} and J are calculated using absorbing boundary conditions, i.e. $\mathcal{W}(s_a, t; s_0, 0) = \mathcal{W}(s_b, t; s_0, 0) = 0$, and where the initial condition implies $\mathcal{W} = \delta(s - s_0)$ at $t = 0$. This represents the probability per unit time that the polymer reaches the boundary at $s = s_b$. The probability that the system reaches s_b first at any time is given by

$$p_b = \int_0^\infty P(\tau) d\tau, \quad (4)$$

and the normalized probability distribution is given by

$$g(\tau; s_0) = P(\tau)/p_b. \quad (5)$$

Finally, the associated mean first passage time is given by

$$\langle \tau \rangle = \int_0^\infty d\tau \tau g(\tau; s_0). \quad (6)$$

Similar relations can be obtained to describe translocation to the other boundary.

In this study, we use free energy functions obtained from MC simulations to solve Eq. (1) and (2) subject to absorbing boundaries at $s = 0$ and $s = N - 1$. This is used to calculate the mean first passage time distributions in Eqs. (3) and (5), as well as the mean first passage time using Eq. (6) and the translocation probability using Eq. (4). We use numerical integration methods, as described in the following section.

IV. METHODS

Monte Carlo simulations employing the Metropolis algorithm and the self-consistent histogram (SCH) method⁴⁶ were used to calculate the free energy functions for the polymer-nanopore model described in Section II. The SCH method provides an efficient means to calculate the equilibrium probability distribution $\mathcal{P}(s)$, and thus its corresponding free energy function, $F(s) = -k_B T \ln \mathcal{P}(s)$. We have previously used this procedure to measure free energy functions in other simulation studies of polymer translocation^{32,33,45} as well in a study of polymer segregation under cylindrical confinement.⁴⁷

To implement the SCH method, we carry out many independent simulations, each of which employs a unique “window potential” of a chosen functional form. The form of this potential is given by:

$$W_i(s) = \begin{cases} \infty, & s < s_i^{\min} \\ 0, & s_i^{\min} < s < s_i^{\max} \\ \infty, & s > s_i^{\max} \end{cases} \quad (7)$$

where s_i^{\min} and s_i^{\max} are the limits that define the range of s for the i -th window. Within each “window” of s , a

probability distribution $p_i(s)$ is calculated in the simulation. The window potential width, $\Delta s \equiv s_i^{\max} - s_i^{\min}$, is chosen to be sufficiently small that the variation in F does not exceed a few $k_B T$. Adjacent windows overlap, and the SCH algorithm uses the $p_i(s)$ histograms to reconstruct the unbiased distribution, $\mathcal{P}(s)$. The details of the histogram reconstruction algorithm are given in Ref. 46. A description for an application to a physical system comparable to that studied here is presented in Ref. 32.

Polymer configurations were generated carrying out single-monomer moves using a combination of translational displacements and crankshaft rotations. The trial moves were accepted with a probability $p_{\text{acc}} = \min(1, e^{-\Delta E/k_B T})$, where ΔE is the energy difference between the trial and current states. Initial polymer configurations were generated such that s was within the allowed range for a given window potential. Prior to data sampling, the system was equilibrated. As an illustration, for a $N = 121$ polymer chain, the system was equilibrated for typically $\sim 10^7$ MC cycles, following which a production run of $\sim 10^8$ MC cycles was carried out. During each MC cycle a move for each monomer is attempted once, on average.

The windows are chosen to overlap with half of the adjacent window, such that $s_i^{\max} = s_{i+2}^{\min}$. The window width was typically $\Delta s = \sigma$. Thus, a calculation for $N = 121$, where the translocation coordinate spans a range of $s \in [0, 120]$, required separate simulations for 239 different window potentials. For each simulation, individual probability histograms were constructed using the binning technique with 10 bins per histogram.

The free energy functions obtained from the MC simulations were used with the procedure summarized in Sec. III to study the translocation dynamics under the assumption that conformational quasi-equilibrium is maintained during the process. The translocation probability $\mathcal{W}(s, t; s_0, 0)$ was determined by solving Eq. (1) for a chosen value of s_0 . Typically, we used $s_0 = L/(2\sigma)$, at which point the first monomer is just on the verge of exiting the pore into the cavity. The equation was solved using standard numerical methods with a “spatial” grid size of $\Delta s = 0.01$ and a time increment of $\Delta t = 0.002\mathcal{D}^{-1}$. The distribution $P(\tau)$ was calculated using Eq. (3), where a standard five-point method was used to evaluate the derivatives in Eq. (2). The translocation probability, p_b , and mean first passage time, $\langle \tau \rangle$, were calculated by numerical integration of Eqs. (4) and (6), respectively, using Simpson’s rule.

In the results presented below, quantities of length are measured in units of σ , energy in units of $k_B T$, force in units of $k_B T/\sigma$ and time in units of \mathcal{D}^{-1} .

V. RESULTS

We consider first the case of spherical cavities in the absence of a driving force or adsorption potential, i.e.

$r = 1$, $f_d = 0$ and $\epsilon = 0$. Figure 2 shows free energy functions for cavity volumes of $V=150, 250$ and 500 , each for polymer lengths ranging from $N=31$ to $N=141$. As expected, the free energy cost of confining the polymer in the cavity increases as the confinement volume decreases. In addition, the curves all have positive curvature everywhere except at near the upper and lower bounds. This indicates that free energy cost of inserting each monomer into the cavity increases as the number (and hence density) of monomers inside increases. This feature is consistent with results from previous MC studies^{27,32,33} and theoretical studies^{16,26} that explicitly account for repulsion between monomers, in contrast to the case for ideal polymers.¹⁵ Another noteworthy feature is the strong degree of overlap between the curves for different N and the same V . Thus, the free energy cost of transferring one monomer from the outside to the inside of the cavity depends approximately only on the density of monomers in the cavity. Deviations from this trend are evident where F dips abruptly near $s = N - 1$.

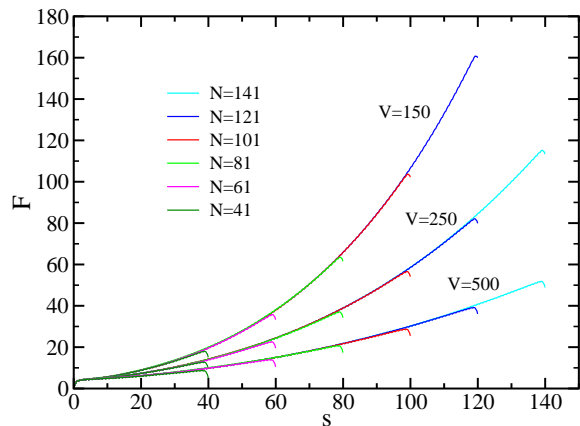


FIG. 2. Free energy functions for several different polymer lengths for a cavity aspect ratio of $r = 1$. Results for three different cavity volumes are shown.

To provide a quantitative analysis of the free energy functions, we employ a standard scaling theory approach.²³ We first recall that the standard form of the entropic free energy barrier for translocation of a polymer through a narrow pore in a flat wall of negligible thickness is $F_0/kT = (1 - \lambda) \ln[m(N - m)]$, where m segments lie on one side of the pore, and $N - m$ lie on the other and where $\lambda = 0.69$ is a critical exponent.¹ This expression can easily be modified to account for the case of a channel in a wall of finite thickness.⁴⁵ To account for the effect of confinement of the monomers inside the cavity, we consider the case where this part of the polymer is in the semi-dilute regime. Here, the confined portion of the polymer can be viewed as a collection n_b blobs, each of size $\xi \sim \sigma \phi^{\nu/(1-3\nu)}$, where ν is the Flory exponent. It is easily shown that the confinement free energy scales as²³ $\Delta F_c/kT = n_b \approx (V/\sigma^3)^{-1/(3\nu-1)} m^{3\nu/(3\nu-1)}$, where

m is the number of monomers in the cavity. For a finite length nanochannel that is spanned by an average of n_p bonds, we note that $m = s - n_p/2$. For the pore length $L = 1.3$ used here, we estimate $n_p = 2$ when the pore is filled. Thus, the total free energy, F , is expected to satisfy

$$(F - F_0)/kT \approx (V/\sigma^3)^{-1.25}(s - n_p/2)^{2.25}, \quad (8)$$

where we have used $\nu = \frac{3}{5}$. This approximation is valid when $n_p/2 < s < N - 1 - n_p/2$. Over most of the range of s , n_p is constant, the logarithmic term F_0 is negligible. Only near the upper and lower bounds of s is the variation of F_0 appreciable. This feature, as well as a partial emptying of the pore, accounts for the dips in F near $s = N - 1$. Otherwise F is dominated by the confinement free energy of the cavity. In the case of fixed V , F is predicted to increase with s independent of the polymer length N . In addition, the variation of F with s has positive curvature, and F increases with decreasing V . These predictions are qualitatively consistent with the data.

The use of the semi-dilute approximation to estimate free energy of confinement in the cavity is expected to be valid only over a restricted range of densities. In Ref. 48 it was shown that the predictions are valid only up to packing fractions of $\phi \approx 0.15$, where $\phi \equiv \pi N \sigma^3 / 6V$. Beyond this value the number of monomers per blob is unacceptably low. A lower limit on ϕ is imposed by the condition that the number of blobs, $n_b = N \phi^{1/(3\nu-1)}$, be sufficiently large. For the polymer lengths considered in this work, it is difficult to find a range of s that satisfies both conditions simultaneously. To analyze the data, we use a more relaxed condition for low density and consider the case where $n_b \geq 3$.

Figure 3 shows the results of fits using Eq. (8) for $N = 121$ and various cavity volumes. The free energy functions have been shifted by $F_0(s)$, which is the free energy function for a flat wall that was calculated explicitly by simulation. We use a fitting function of the form $F - F_0 = c_0 + c_1(s - 1)^{-\alpha}$. The lower limit of the range of the fit is indicated in the plot, while the fitting function is deliberately extrapolated beyond the upper limit of the fitting range to illustrate the divergence of the prediction from the simulation results at high density. The upper limit itself is explicitly labeled for two of the functions. Note that scaling predictions underestimate the free energy in the region where $\phi \geq 0.15$. This is consistent with the observation noted in Ref. 48 that the confinement free energy crosses over into a concentrated regime where the excluded volume interactions are screened, which leads to a higher value of α . From the fit to the data in the valid range, it was found that $\alpha=1.9$, 2.0 and 1.9 for $V=150$, 250 and 500, respectively. This is somewhat below the predicted value of $\alpha = 2.25$. Noting the expected dependence of $c_1 \propto V^{-\beta}$ where $\beta=1.25$, the ratio of c_1 measured for $V=500$ and $V=250$ yields $\beta = 0.9$, while the ratio for $V=500$ and $V=150$ yields $\beta=1.1$. Thus, the measured values of the exponents α

and β both deviate from the predicted values. Undoubtedly, this arises from failing to properly satisfy the condition that $n_b \gg 1$. We speculate that better satisfying this condition would yield improved agreement. However, this would necessitate using polymer chains at least an order of magnitude larger than those considered here, which is not feasible for us at present.

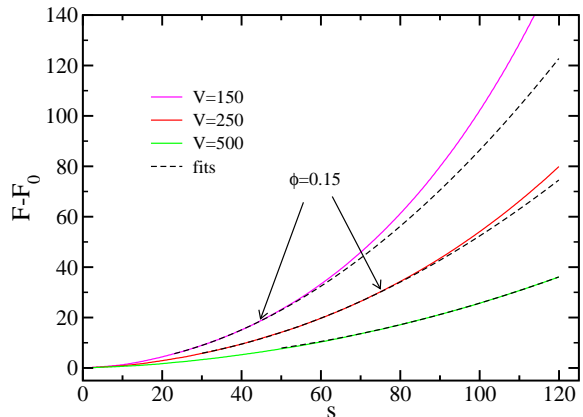


FIG. 3. Free energy functions for polymers of length $N = 121$ and a spherical cavity of various volumes. The dashed black lines show fits to the data in the region for which $n_b \geq 3$ and $\phi < 0.15$. The lower limit of this range is evident from the minimum s for the fitting curves, and the upper end of this range is explicitly labeled for two of the curves. For $V=500$, the upper limit extends beyond the range of the data.

Next we consider the effects of the anisometry of the confining cavity. Figure 4 shows free energy functions for chains of length $N = 101$ in a cavity of volume $V = 500$. Figure 4(a) shows results for prolate ellipsoidal cavities ($r > 1$) and Fig. 4(b) shows results for oblate cavities ($r < 1$). In each case, the result for spherical cavities is also shown, for comparison. The most notable feature here is the fact that deviations from spherical symmetry in either direction lead to an increase in the free energy. Note, however, that the curves for oblate cavities follow the opposite trend at low s (see the inset of Fig. 4(b)), in contrast to the case for prolate cavities. The explanation for this difference is straightforward. As the first few monomers enter the cavity, the effects of confinement are felt mainly by the curvature of the cavity wall near the pore. As the cavity becomes more prolate, this local curvature increases, reducing the number of chain configurations, and F increases, accordingly. By contrast, as the cavity becomes increasingly oblate, the local curvature decreases, leading to slight initial reduction of F with decreasing r evident in the figure. As more monomers enter the cavity the polymer feels the presence of the cavity wall on the side opposite from the pore, and the trend reverses.

Figure 5(a) shows the variation of ΔF with the cavity aspect ratio r , where $\Delta F \equiv F(N - 1) - F(0)$. Results are shown for three different cavity volumes. For

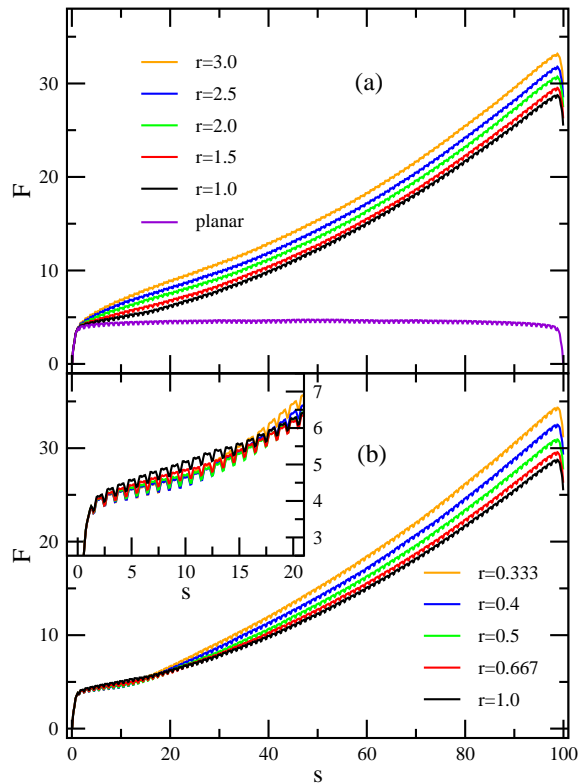


FIG. 4. Free energy functions for a polymer of length $N = 101$ and a ellipsoidal cavity volume of $V = 500$. No driving force is present. Results for several different cavity aspect ratios are shown. The graph in (a) shows results for prolate cavities and (b) shows results for oblate cavities. For comparison, the function F_0 for planar wall geometry is shown in (a). The inset for (b) shows a close-up of the curves at low s .

$V = 500$, ΔF is a minimum for spherical cavities, as was noted from the results of Fig. 4. In addition, ΔF is approximately symmetrical about $r = 1$ in the sense that $\Delta F(r) \approx \Delta F(1/r)$, though oblate side is slightly higher. For a lower cavity volume of $V = 250$, the trend persists, though with a weaker dependence of ΔF with r . For the lowest cavity volume considered, $V = 150$, there is negligible variation of ΔF with r . Thus, the anisotropy of the cavity affects the confinement free energy in the cavity only at moderate densities, while at high densities no effect is observable.

Figure 5(b) shows mean first passage translocation times, $\langle \tau \rangle$, for ejection of the polymer from the cavity. The results were obtained employing the FP formalism described earlier, using the calculated free energy functions. As expected, $\langle \tau \rangle$ is a maximum for $r=1$ for $V=500$ and 250, and shows the same approximate symmetry about $r=1$ as observed in (a). The dependence of $\langle \tau \rangle$ with r does lessen slightly as V decreases. Surprisingly, however, the maximum of $\langle \tau \rangle$ at $r=1$ remains appreciable even at $V = 150$, in spite of the corresponding result

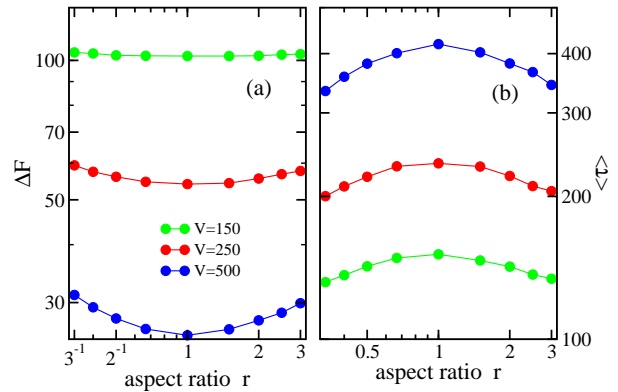


FIG. 5. (a) Free energy difference, $\Delta F \equiv F(N - 1) - F(0)$, vs ellipsoidal cavity aspect ratio, r . Results are shown for $N=101$ for three different cavity volumes. No driving force is present. (b) Mean translocation time, $\langle \tau \rangle$, vs r .

for ΔF . To understand this apparent discrepancy, let us compare the free energy functions for $r=1$ and $r=3$ at each of the volumes considered. The curves are shown in Fig. 6. While the variation in ΔF with r decreases with cavity volume, the free energy remains appreciably higher for the prolate cavity over most of the range of s . This corresponds to a somewhat higher average curvature of F for the spherical cavity. Evidently, it is this feature that leads to the observed difference in $\langle \tau \rangle$. Figure 6(b) shows the full translocation time distributions obtained from the FP formalism, where the persistence of the shift toward slower translocation for aspherical cavities for smaller cavity volumes is clear. Note that the reduction of the ejection time with increasing cavity anisotropy is consistent with the results of the Langevin dynamics study of Ref. 20.

Next, we examine the effect of the variation of ΔF with the cavity asymmetry upon changes in the polymer length. For a polymer at $s=N-1$, there are $N-2$ bonds inside the cavity (one is still confined in the pore). Thus, $\Delta F/(N-2)$ is the confinement free energy per bond inside the cavity at this point. The inset of Fig. 7 shows the N -dependence of $\Delta F/(N-2)$. Results are shown for three different cavity volumes, each with $r=1$ and $r=3$. Several trends are evident. First, for a cavity of fixed volume, the free energy per bond increases with N , and it decreases with V . This follows from the fact that longer chains and smaller volumes correspond to higher packing densities inside the cavity. The other notable trend is that the confinement free energies for the prolate and spherical cavities are appreciably different at low N but tend to converge at high N . The convergence is stronger for smaller V . To clarify this trend, Fig. 7 shows the ratio of ΔF for $r=3$ and $r=1$ plotted as a function of ϕ , the packing fraction in the cavity at $s = N - 1$. Though the curves for each V do not overlap, they do follow the same overall pattern: the ratio decreases monotonically

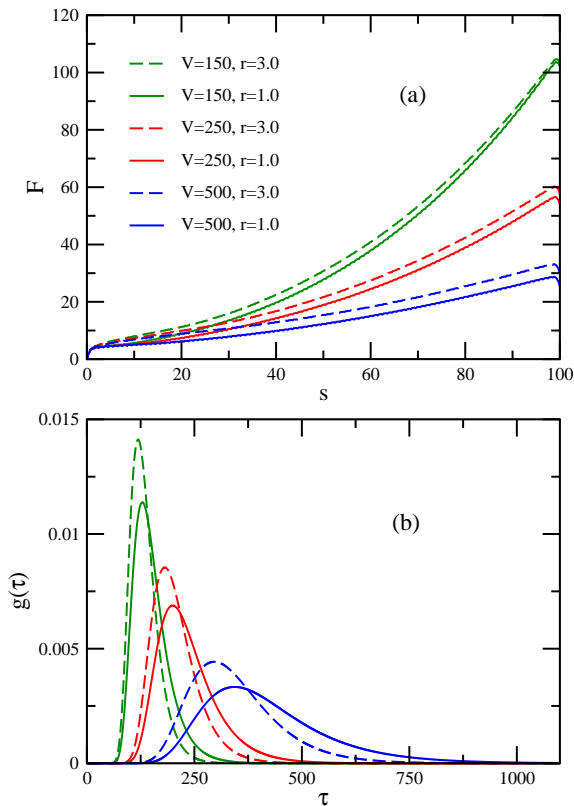


FIG. 6. (a) Free energy vs functions for a polymer of length $N = 101$. Data are shown for three different cavity volumes, each for spherical ($r = 1$) and prolate ($r = 3$) shapes. In all cases, the driving force is zero. (b) Translocation time distributions calculated by numerically solving the FP equation and employing the free energy functions shown in (a).

toward unity as ϕ increases. The same trend was found for oblate ($r = 1/3$) cavities, as well (data not shown). Thus, the anisotropy of the cavity has negligible effect on the confinement free energy at high density.

As noted in Ref. 48, the confinement free energy of a polymer under triaxial confinement scales as $\Delta F_c \sim \phi^{\nu/(1-3\nu)}$ in the semi-dilute regime, which crosses over to $\Delta F_c \sim N\phi^2$ at higher density. In neither case does the expression depend on the shape of the confining cavity. However, these approximations likely require sufficiently large volumes to apply. In the former case, the number of blobs is assumed to be large, implying that the blob dimension ξ is small relative to the confinement dimensions. As ϕ decreases, ξ increases, and the required condition becomes more poorly satisfied. This, in part, may explain the trend observed in Fig. 7. Clarification of these effects will require results from simulations employing much longer polymer chains.

Next, we consider the effect of a driving force acting on monomers inside the pore to push the polymer into the cavity. These calculations do not require additional sim-

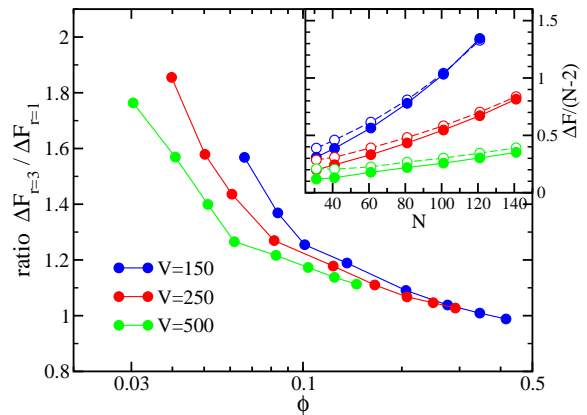


FIG. 7. Ratio of ΔF for $r = 3$ and $r = 1$ vs maximum packing fraction, ϕ . Data are shown for polymer lengths in the range $N=31$ – 141 and cavity volumes of $V = 150, 250$ and 500 , each with aspect ratios of $r = 1$ and 3 . The inset shows the scaled free energy barrier heights, $\Delta F / (N - 2)$, vs polymer length, N . Solid symbols correspond to $r = 1$ and open symbols correspond to $r = 3$.

ulations. To an excellent approximation, the free energy function for finite f_d is given by

$$F(s; f_d) = F(s; 0) - f_d L s \quad (9)$$

Thus, previous results for $f_d = 0$ can be easily modified to yield free energy functions for finite f_d . A few simulations with a finite driving force were carried out, and the validity of this expression was confirmed (data not shown).

To study the effect of varying V and r on $F(s)$ and the translocation rate, it is helpful to introduce a modified driving force, defined $f'_d \equiv f_d - \Delta F(f_d = 0) / [L(N - 1)]$. Note that $f'_d = 0$ corresponds to the case where $F(0) = F(N - 1)$ for arbitrary f_d and V . The shift is designed to examine the combined effect of the driving force and the curvature of $F(s)$ in the absence of the entropic bias toward polymer ejection.

Figure 8 shows results for polymers of length $N = 101$ in a cavity of volume $V=150$ and $V=500$. Data are shown for several different driving forces, each for the case of a spherical cavity and a prolate ($r=3$) cavity. The free energy curves in Fig. 8(a) are also labeled with f'_d . The curves in Fig. 8(b) for $V=500$ correspond to specific values of f'_d . For $V=500$, note that $r=1$ and $r=3$ curves with the same f'_d correspond to different f_d , since $\Delta F(f_d = 0)$ differ for different r , as was evident in Fig. 6(a). The main effect of the driving force is to remove the free energy penalty for inserting the polymer into the cavity. This point is first reached when $f'_d=0$ (i.e. $f_d = \Delta F(f_d = 0) / [L(N - 1)]$.) Beyond that point F is lower for the polymer completely inside than where it is completely outside. As shown for $V=150$ in Fig. 8(a), increasing f_d generally increases rate that F

decreases with s . However, the magnitude of dF/ds decreases with s , which is a consequence of the curvature of $F(s)$ for $f_d=0$. In addition, for moderate values of f_d , the function exhibits a local minimum when the polymer is mostly inside the cavity. For example, for $f_d=1.3$, the minimum lies at $s_{\min} \approx 80$, as is clear from the inset of the figure. The magnitude of the resulting barrier between s_{\min} and $s = N - 1$ decreases and eventually vanishes about some critical value of f_d . The presence of such a minimum has been noted in previous studies of translocation into spherical cavities with a driving force arising from attraction of monomers to the cavity walls,^{26,27} and effective forces arising from translocation between cavities of different sizes.¹⁶

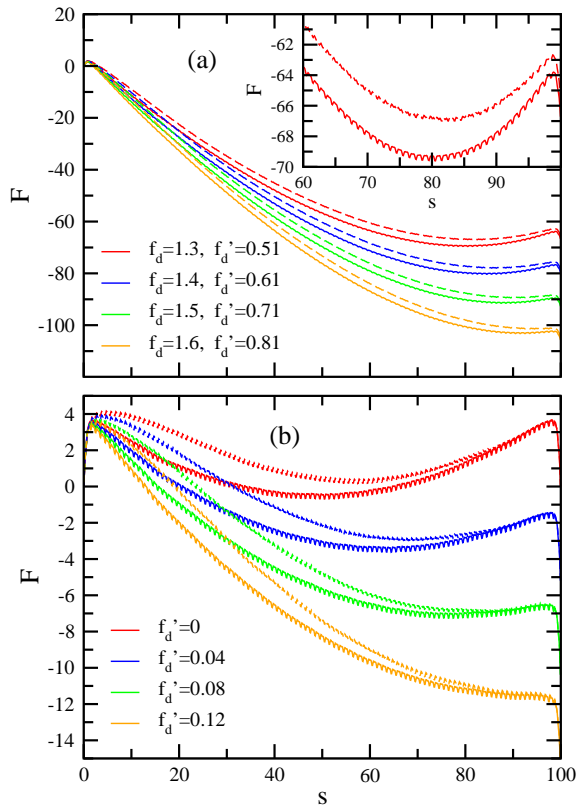


FIG. 8. Free energy functions for a polymer of length $N=101$ and a cavity of volume $V=150$ in (a) and $V=500$ in (b). Results are shown for several f_d and/or f'_d , where the shifted driving force f'_d is defined in the text. Solid curves correspond to spherical cavities (i.e. $r=1$) and dashed curves are shown for prolate cavities with $r=3$. The inset in (a) shows a close-up of the curves for $f_d=1.3$.

As noted earlier, $\Delta F (\equiv F(N-1) - F(0))$ is approximately invariant with respect to r for $N=101$ and $V=150$ in the case where $f_d=0$. From Eq. (9) it follows that this is also true for arbitrary f_d . However, over most of the range of s , there is an appreciable dependence of $F(s)$ on r . This is evident in Fig. 8(a), which illustrates the difference in the curves for the cases of $r=1$ and $r=3$.

Unlike the case illustrated in Fig. 6 for $f_d=0$, where the anisotropy of the cavity has a small effect on the rate for polymer ejection, small changes in r can have a significant effect on the rates of polymer insertion.

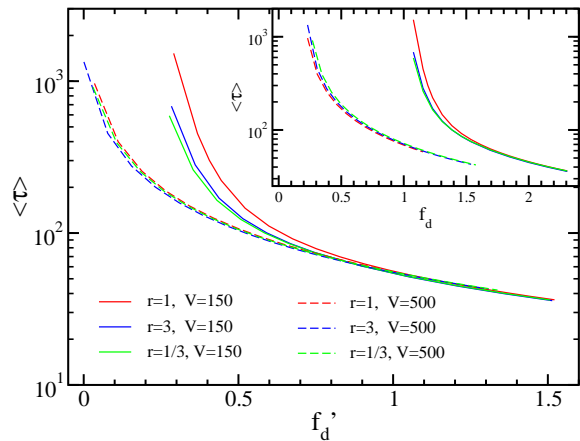


FIG. 9. Mean translocation time $\langle \tau \rangle$ vs shifted driving force, f'_d , where $f'_d \equiv f_d - \Delta F(f_d = 0)/(L(N-1))$. Results are shown for a polymer of length $N=101$ for cavity volumes of $V=150$ and $V=500$, each for three different cavity aspect ratios. The inset shows the same results plotted as a function of the driving force, f_d .

The effects of the free energy functions on the polymer insertion translocation times are illustrated in Figure 9, which shows results for translocation times calculated using the FP method for $N=101$ and volumes of $V=150$ and $V=500$, each for cavity anisotropies of $r=1/3$, 1, and 3. The inset shows $\langle \tau \rangle$ vs f_d . As expected, the translocation times decrease with increasing f_d . In addition, the translocation rate is faster when the cavity volume is larger. This follows from the fact that the entropic force acting against f_d is greater for smaller volumes, as was noted in Fig. 6(a). The main part of the figure shows $\langle \tau \rangle$ vs f'_d . At large f'_d , the translocation times all converge to the same curve. In this regime, effects of the curvature of $F(s)$ become negligible, and the translocation rate is governed principally by dF/ds . For any given value of f'_d , $dF/ds \approx f_d$ independent of V , and so $\langle \tau \rangle$ will be equal. At lower values of f'_d , the results for the two volumes diverge. The curves for $V=150$ begin to increase rapidly near $f'_d \approx 0.5$ and those for $V=500$ diverge near $f'_d \approx 0.1$. In each case, the rapid increase in $\langle \tau \rangle$ is due to the increasing influence of the curvature of $F(s)$ as the driving force decreases. The curvature gives rise to the free energy minimum evident in Fig. 8 and the associated free energy barrier. As was clear in Fig. 6(a), the curvature of the function is greater when the cavity volume is lower. Thus, the onset of the rapid increase in $\langle \tau \rangle$ occurs first for $V=150$. For this volume, the free energy minimum first appears around $f_d \approx 1.5$, and deepens rapidly as f_d increases. As seen in Fig. 8, this corresponds to $f'_d \approx 0.7$.

By contrast, the free energy minimum for $V=500$ appears at $f'_d \approx 0.1$. Both of these results are consistent with the trends in the figure.

Finally, we consider the effects of cavity anisotropy on the translocation times. At high f_d , it is clear that varying r has negligible effect on $\langle \tau \rangle$. In this limit, $F(s) \approx -f_d L s$, which is independent of r , and so the invariance of $\langle \tau \rangle$ to r is expected. For $V=150$, a different trend emerges at lower f_d , where the free energy minimum emerges. In this regime, $\langle \tau \rangle$ becomes greater for spherical cavities than for either prolate or oblate cavities. For example, for $f_d = 1.15$, $\langle \tau \rangle$ is 1.6 times greater for $r=1$ than for $r=3$. This effect is not present for $V=500$. Thus, shape anisotropy of the cavity leads to faster polymer insertion at low driving force and high packing fraction. This can be understood from inspection of Fig. 8(a), where we observe a deeper free energy minimum for $r=1$ than for $r=3$. This trend persists for functions with lower f_d than those values shown in figure. In the case of $V=500$, there appears to be negligible effect of the anisotropy on $\langle \tau \rangle$. From the arguments above, there is expected to be some effect in the regime where a free energy minimum is present. From Fig. 8(b), this occurs for $f'_d \lesssim 0.1$. However, we note that the difference in the depths of the minima for $r=1$ and $r=3$ is $\lesssim kT$. By contrast, the difference is considerably greater for $V=150$ at some positive values of f'_d . Consequently, the effects of the cavity anisotropy are expected to be more appreciable for smaller V , in accord with the results.

The translocation time predictions can be compared with the results of the Langevin dynamics simulation study of Ali *et al.*²⁰ They studied ejection and insertion of flexible and semi-flexible polymers of length $N = 100$ for a prolate ellipsoidal cavity of comparable dimensions to the $V = 150$ cavity considered here, as well as for a spherical cavity of the same volume. In the case of ejection of a flexible polymer, they found faster translocation for ellipsoidal cavities, in agreement with the results presented earlier. However, for insertion of a flexible polymer, they found that translocation was faster for the spherical cavity. Those results are in disagreement with our predictions. Most likely, this is due to out-of-equilibrium conformational behaviour in the dynamics simulations. Such effects are not accounted for in the FP approach, which assumes quasistatic dynamics. The predictions are also in disagreement with the 2-D Langevin dynamics study in Ref. 31, where insertion proceeded most rapidly in the case of a circular cavity, independent of packing fraction. In this case, it is less clear whether the discrepancy arises from nonequilibrium dynamics or from a different underlying behaviour of the free energy for 2-D. Regardless, these results demonstrate the need to exercise caution in using free energy arguments to interpret translocation simulation results. The assumptions for the valid use of the FP approach are only satisfied for sufficiently high pore friction, as we noted in Refs. 33 and 45. However, such predictions are useful for identifying some of the qualitative effects of nonequilibrium dynamics.

The final case we consider in this study is translocation into an adsorbing cavity. Here, monomers have an energy of $-\epsilon$ if their centers lie within a distance σ ($=1$) from the elliptical surface of the cavity. Figure 10 shows free energy functions for various values of ϵ for a polymer of length $N=101$. Results are shown in (a) for a cavity volume of $V = 150$ and in (b) for $V=500$, each for cavity anisotropies of $r=1$ and 3. As expected, increasing the attraction to the cavity wall decreases ΔF , and thus removes the entropic cost of insertion of the polymer into the cavity. Generally, the free energy function has positive curvature. Beyond some value of ϵ , we see that $\Delta F < 0$, i.e. it is more favourable for the polymer to lie completely inside rather than completely outside the cavity. However, there is an intermediate range of ϵ for which there is a local free energy minimum and thus a free energy barrier that must be overcome for complete insertion. The depth of the free energy minimum is greater in the cavity with the smaller volume. These trends are qualitatively comparable to those for the curves shown in Fig. 8 for the case of a driving force in the nanopore. In addition, the curves are qualitatively similar to those calculated in Refs. 26 and 27 for adsorbing spherical cavities. Note that the details of the model employed in those studies differed from the present model, and thus a direct quantitative comparison of the results is not possible.

For each ϵ value, the free energy curve for the prolate cavity lies above that for the spherical cavity. The results for oblate cavities with $r=1/3$ were comparable to those of $r=3$ (data not shown). Thus, increasing the anisotropy of the cavity reduces the effectiveness of the attraction to the cavity wall to drive the polymer into the cavity. This general result is also clear in the inset of Fig. 10(a), which shows ΔF vs ϵ . Comparing with Fig. 8, we note that the cavity anisotropy has the same effect on the free energy for the case of attractive cavity walls as it did for the case of a driving force acting in the pore. However, the differences between the free energies for spherical and anisometric cavities are greater in the present case, and increase with increasing ϵ . Comparing the results in Fig. 10(a) and (b), we find that the absolute degree to which the curves are shifted between $r=1$ and $r=3$ is not significantly affected by the cavity volume.

Translocation time distributions calculated using the FP formalism and the free energy functions in Fig. 10(b) are illustrated for $N=101$ and $V=500$ in Fig. 11. Results are shown for values of ϵ that are sufficiently large for an appreciable probability that the polymer is driven into the cavity. As expected from the free energy functions, increasing the cavity anisotropy significantly slows down the rate of insertion. By contrast, cavity anisotropy has a negligible effect on the polymer insertion rate for cavities of the same volume in the case where insertion is driven by a force acting in the nanopore, as was evident in Fig. 9. The strong effect observed here apparently arises from the fact that changing the shape of the cavity distorts the polymer in a way that reduces the average

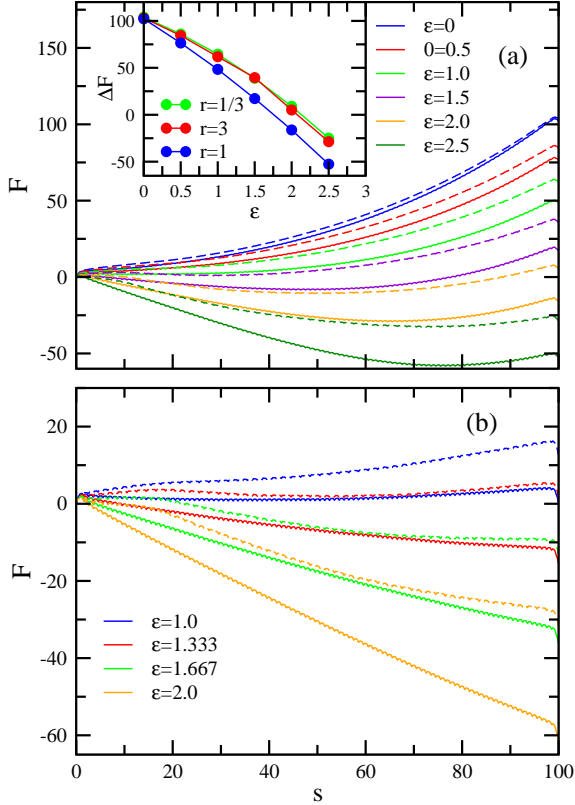


FIG. 10. Free energy functions for an adsorbing cavity for various adsorption strengths for a polymer of length $N=101$. Results in (a) are for $V=150$ and (b) are for $V=500$. The solid curves are for spherical ($r=1$) cavities, and the dashed curves are for prolate ($r=3$) cavities. The inset in (a) shows the free energy difference $\Delta F \equiv F(N-1) - F(0)$ vs ϵ .

number of monomer-surface contacts in the cavity for the accessible conformations. For the model with the driving force in the nanopore, this kind of effect does not affect the energetic contribution to the free energy, unlike the case where surface interactions are present.

VI. CONCLUSIONS

In this study, we have used simulation and theoretical methods to investigate the translocation of a flexible hard-sphere polymer into and out of an ellipsoidal cavity. Monte Carlo simulations were employed to calculate translocation free energy functions, and these functions were used together with the Fokker-Planck equation to predict the translocation times. We considered the case of ejection from the cavity for an athermal system, as well as the case of polymer insertion driven either by a force acting in the pore or by monomer attraction to the walls of the cavity. We studied the effects on the free energy and predicted dynamics of varying all of the rel-

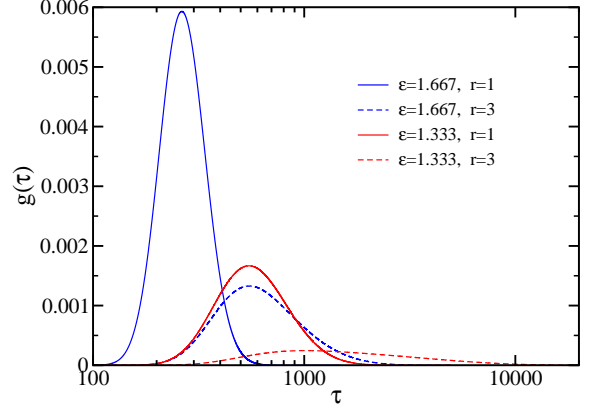


FIG. 11. Translocation time distributions for systems with an attractive cavity wall, for $N=101$ and $V=500$. Results for two values of ϵ are shown, each for cavity aspect ratios of $r=1$ and $r=3$.

evant system parameters, with special attention to the effect of the cavity anisotropy.

The free energy functions calculated for the athermal system with spherical cavities are consistent with those calculated previously by analytical methods¹⁶ and by simulation.^{27,32} We find that the variation of F with packing fraction is approximately consistent with a scaling theory prediction that treats the polymer to be in the semi-dilute regime inside the cavity. Deviations from the predicted scaling exponents likely arise from finite-size effects. Increasing the anisotropy of the cavity at fixed volume increases the free energy cost of insertion. The effect is approximately symmetric with respect to prolate or oblate distortions and diminishes with increasing cavity packing fraction. This increase in the free energy leads to a prediction of faster polymer ejection for ellipsoidal cavities compared to spherical cavities. This is consistent with the ejection rates measured in a previous Langevin dynamics simulation study.²⁰ Application of a driving force on monomers in the pore leads to a local free energy minimum for an intermediate range of force magnitudes, and the corresponding free energy barrier slows the insertion. Increasing the shape anisotropy of the cavity causes faster polymer insertion at high packing fractions and moderate driving force, but has negligible effect for larger cavities or high driving force. This result is inconsistent with Ref. 20, most likely because of out-of-equilibrium conformational behaviour that is not accounted for in the FP approach. Finally, the translocation rate for insertion driven by monomer attraction to the cavity walls is much more sensitive to cavity anisotropy than for the case of insertion driven a force in the pore.

It is intriguing that the predicted qualitative effects of the cavity shape on translocation rate are in agreement with observations from dynamics simulations for ejection

but not insertion. As noted, the latter discrepancy is due to nonequilibrium behaviour, most likely associated with the encapsulated part of the polymer, which provides the dominant contribution to the free energy function. The internal dynamics of this portion likely becomes very sluggish at high densities. Increasing the cavity anisotropy at fixed volume narrows the cavity in at least one dimension, leading perhaps to slower conformational rearrangement and an increase in nonequilibrium effects. However, it seems likely that the ejection process would also exhibit this behaviour as well for the same simulation model. Evidently, there is a hysteresis effect at play here, which was also noted in Ref. 20. In future work, we will examine this issue further and quantify the deviation from equilibrium behaviour by carrying dynamics simulations for variable pore friction. At high pore friction, the polymer ejection dynamics are perfectly consistent with FP predictions,³³ and it is likely to be the case for insertion as well. This work should contribute to understanding the limits of the validity of employing free energy arguments to understand DNA ejection and packaging in viruses, as well as other systems, where nonequilibrium effects are appreciable.

ACKNOWLEDGMENTS

This work was supported by the Natural Sciences and Engineering Research Council of Canada (NSERC). We are grateful to the Atlantic Computational Excellence Network (ACEnet) for use of their computational resources.

- ¹M. Muthukumar, *Polymer Translocation* (CRC Press, Boca Raton, 2011).
- ²S. Carson and M. Wanunu, *Nanotechnology* **26**, 074004 (2015).
- ³L. J. Steinbock and A. Radenovic, *Nanotechnology* **26**, 074003 (2015).
- ⁴M. Wanunu, *Phys. Life Rev.* **9**, 125 (2012).
- ⁵B. M. Venkatesan and R. Bashir, *Nat. Nanotech.* **6**, 615 (2011).
- ⁶R. Stefureac, L. Waldner, P. Howard, and J. S. Lee, *Small* **4**, 59 (2008).
- ⁷C. C. Striemer, T. R. Gaborski, J. L. McGrath, and P. M. Fauchet, *Nature* **445**, 749 (2007).
- ⁸P. Yang, S. Gai, and J. Lin, *Chemical Society Reviews* **41**, 3679 (2012).
- ⁹B. Alberts, A. Johnson, J. Lewis, M. Raff, K. Roberts, and P. Walters, *Molecular Biology of the Cell*, 5th ed. (Garland Science, New York, 2008).
- ¹⁰H. Lodish, A. Berk, C. A. Kaiser, M. Krieger, A. Bretscher, H. Ploegh, A. Amon, and M. P. Scott, *Molecular Cell Biology*, seventh ed. (W. H. Freeman and Company, New York, 2012).
- ¹¹A. Milchev, *J. Phys.: Condens. Matter* **23**, 103101 (2011).
- ¹²D. Panja, G. T. Barkema, and A. B. Kolomeisky, *J. Phys.: Condens. Matter* **25**, 413101 (2013).
- ¹³V. V. Palyulin, T. Ala-Nissila, and R. Metzler, *Soft matter* **10**, 9016 (2014).
- ¹⁴M. Muthukumar, *Phys. Rev. Lett.* **86**, 3188 (2001).
- ¹⁵M. Muthukumar, *J. Chem. Phys.* **118**, 5174 (2003).
- ¹⁶C. Y. Kong and M. Muthukumar, *J. Chem. Phys.* **120**, 3460 (2004).
- ¹⁷I. Ali, D. Marenduzzo, and J. Yeomans, *J. Chem. Phys.* **121**, 8635 (2004).
- ¹⁸I. Ali, D. Marenduzzo, C. Micheletti, and J. Yeomans, *J. Theor. Med.* **6**, 115 (2005).
- ¹⁹A. Cacciuto and E. Luijten, *Phys. Rev. Lett.* **96**, 238104 (2006).
- ²⁰I. Ali, D. Marenduzzo, and J. Yeomans, *Phys. Rev. Lett.* **96**, 208102 (2006).
- ²¹C. Forrey and M. Muthukumar, *Biophys. J.* **91**, 25 (2006).
- ²²I. Ali, D. Marenduzzo, and J. Yeomans, *Biophys. J.* **94**, 4159 (2008).
- ²³T. Sakaue and N. Yoshinaga, *Phys. Rev. Lett.* **102**, 148302 (2009).
- ²⁴A. Matsuyama, M. Yano, and A. Matsuda, *J. Chem. Phys.* **131**, 105104 (2009).
- ²⁵I. Ali and D. Marenduzzo, *J. Chem. Phys.* **135**, 095101 (2011).
- ²⁶S. Yang and A. V. Neimark, *J. Chem. Phys.* **136**, 214901 (2012).
- ²⁷C. J. Rasmussen, A. Vishnyakov, and A. V. Neimark, *J. Chem. Phys.* **137**, 144903 (2012).
- ²⁸S. Ghosal, *Phys. Rev. Lett.* **109**, 248105 (2012).
- ²⁹K. Zhang and K. Luo, *J. Chem. Phys.* **136**, 185103 (2012).
- ³⁰A. Al Lawati, I. Ali, and M. Al Barwani, *PLoS one* **8**, e52958 (2013).
- ³¹K. Zhang and K. Luo, *Soft Matter* **9**, 2069 (2013).
- ³²J. M. Polson, M. F. Hassanabad, and A. McCaffrey, *J. Chem. Phys.* **138**, 024906 (2013).
- ³³J. M. Polson and A. C. McCaffrey, *J. Chem. Phys.* **138**, 174902 (2013).
- ³⁴J. Mahalik, B. Hildebrandt, and M. Muthukumar, *J. Biol. Phys.* **39**, 229 (2013).
- ³⁵R. Linna, J. Moisio, P. Suhonen, and K. Kaski, *Phys. Rev. E* **89**, 052702 (2014).
- ³⁶K. Zhang and K. Luo, *J. Chem. Phys.* **140**, 094902 (2014).
- ³⁷Q. Cao and M. Bachmann, *Phys. Rev. E* **90**, 060601 (2014).
- ³⁸K. Luo, R. Metzler, T. Ala-Nissila, and S.-C. Ying, *Phys. Rev. E* **80**, 021907 (2009).
- ³⁹K. Luo and R. Metzler, *Phys. Rev. E* **82**, 021922 (2010).
- ⁴⁰K. Luo and R. Metzler, *J. Chem. Phys.* **134**, 135102 (2011).
- ⁴¹J. Sheng and K. Luo, *Soft Matter* **8**, 367 (2012).
- ⁴²N. Chiaruttini, M. De Frutos, E. Augarde, P. Boulanger, L. Letellier, and V. Viasnoff, *Biophys. J.* **99**, 447 (2010).
- ⁴³Z. T. Berndsen, N. Keller, S. Grimes, P. J. Jardine, and D. E. Smith, *Proc. Natl. Acad. Sci. USA* **111**, 8345 (2014).
- ⁴⁴Y. Kantor and M. Kardar, *Phys. Rev. E* **69**, 021806 (2004).
- ⁴⁵J. M. Polson and T. R. Dunn, *J. Chem. Phys.* **140**, 184904 (2014).
- ⁴⁶D. Frenkel and B. Smit, *Understanding Molecular Simulation: From Algorithms to Applications*, 2nd ed. (Academic Press, London, 2002) Chap. 7.
- ⁴⁷J. M. Polson and L. G. Montgomery, *J. Chem. Phys.* **141**, 164902 (2014).
- ⁴⁸A. Cacciuto and E. Luijten, *Nano Lett.* **6**, 901 (2006).